Geocarto International

ISSN: (Print) (Online) Journal homepage: https://www.tandfonline.com/loi/tgei20

Influence of AGL flight and off-nadir images on UAV-SfM accuracy in complex morphology terrains

Francisco Agüera-Vega, Ezequiel Ferrer-González, Fernando Carvajal-Ramírez, Patricio Martínez-Carricondo, Paolo Rossi & Francesco Mancini

To cite this article: Francisco Agüera-Vega, Ezequiel Ferrer-González, Fernando Carvajal-Ramírez, Patricio Martínez-Carricondo, Paolo Rossi & Francesco Mancini (2022): Influence of AGL flight and off-nadir images on UAV-SfM accuracy in complex morphology terrains, Geocarto International, DOI: 10.1080/10106049.2022.2074147

To link to this article: https://doi.org/10.1080/10106049.2022.2074147

Accepted author version posted online: 09 May 2022.

Influence of AGL flight and off-nadir images on UAV-SfM accuracy in complex morphology terrains

Francisco Agüera-Vega[1,*], Ezequiel Ferrer-González[1], Fernando Carvajal-Ramírez[1], Patricio Martínez-Carricondo[1], Paolo Rossi[2], and Francesco Mancini[2]

[1]Department of Engineering, University of Almería, La Cañada de San Urbano (Mediterranean Research Center of Economics and Sustainable Development (CIMEDES), Agrifood Campus of International Excellence, ceiA3), Almería, Spain

[2]Department of Engineering (DIEF) 'Enzo Ferrari', University of Modena and Reggio Emilia, Modena, Italy

[*]Correspondence: faguera@ual.es

Abstract

In the field of geosciences and engineering, situations arise where special attention have to be paid to the planning of the UAV-photogrammetric project, i.e., terrain with complex geometry and steep slopes. The use of off-nadir imagery and flights at a fixed height above ground level (AGL) are postulated as possible factors to be considered to achieve high accuracies. The objective of this study is to evaluate the influence of image angle, frontal and side overlaps, and type of flight (above mean sea level (AMSL) or AGL), on the accuracy of the dense 3 D point cloud yielded by UAV-SfM. The results obtained showed that imagery with an angle between 20° and 35° in two perpendicular flight line directions, 90/90, 90/70 or 70/70 overlap and AGL flight is the optimal combination for best accuracy and high precision. With nadir imagery, the combination of factors that gives the most accuracy results are AGL flights with a 90/70 overlap.

Keywords unmanned aerial vehicle; oblique images; above ground level; above mean sea level; UAV-SfM photogrammetry; complex terrain morphology

1. Introduction

Unmanned aerial vehicles (UAVs) are widely used platforms to provide high temporal and geometrical resolution data for mapping and modelling for geosciences and engineering purposes (Mancini et al. 2013; Mourato et al. 2017; Rossi et al. 2018; Carvajal-Ramírez et al. 2019; Gong et al. 2019; Ferrer-González et al. 2020; Menegoni et al. 2020; Carricondo et al. 2021). A wide range of sensors can be attached to a UAV, although the most commonly used for mapping purposes are digital cameras, which despite not being metric, have a lightweight and high image quality (Manconi et al. 2019). Furthermore, due to the development of image processing techniques, such as structure from motion (SfM) and multiview stereopsis (MVS), combination of UAVs, SfM and MVS (for the sake of simplicity, this combination will hereafter be referred to as UAV-SfM) offers effective and cost-efficient photogrammetric techniques to obtain a high-resolution data set (Westoby et al. 2012). SfM technique provides a sparse 3 D point cloud in an arbitrary coordinate system and a full camera calibration, solving the collinearity equations without the need for any ground control point (Pérez et al. 2011; Fonstad et al. 2013). This is possible due to image matching algorithms that automatically search for similar image objects (key points) by analysing the correspondence, similarity and consistency of the image features (Ao et al. 2018). SfM paired with MVS yield a dense 3 D point cloud (Furukawa & Ponce 2010).

When the terrain under study is steep and has a complex geometry, it is necessary to pay special attention to the image capture and processing techniques to obtain reliable results (reduce

data gaps and obtain high accuracy) in planimetric and altimetric dimensions. Some of the main considerations in flight planning for UAV-SfM are the flight altitude, camera axis angle regarding the terrain, and the front and side overlap. Together with the sensor dimension, resolution, and focal length, all of these parameters determine the ground sample distance (GSD) and the accuracy of the final results (Manconi et al. 2019). The traditional plan flights in geomorphic applications are formed by parallel lines at a constant altitude, with a pre-defined front and side overlap and a nadir angle of the camera axis (Nesbit & Hugenholtz 2019; James et al. 2020). In the event that the site of study is a vertical or quasi-vertical feature, the flight path lines are oriented in parallel to it, and the camera axis is oriented perpendicular to it (Agüera-Vega et al. 2018; Martínez-Carricondo et al. 2020). However, if the surface under study has complex geometric and interest-oriented features in all directions, this exposed strategy for capturing planning data cannot capture enough detail or geometric information (Rossi et al. 2017). In order to mitigate this problem, the incorporation of oblique images has been proposed in applications related to terrains with complex geometry or steep slopes (Bemis et al. 2014; Harwin et al. 2015; Carvajal-Ramírez et al. 2016; Rossi et al. 2017; Agüera-Vega et al. 2018; Nesbit & Hugenholtz 2019). Furthermore, a combination of nadir and oblique images can produce a more precise self-calibrating bundle adjustment when using nadir images alone due to better internal calibration of the camera (James & Robson 2014; Harwin et al. 2015), which largely determines the accuracy of photogrammetric products. In this regard, (Štroner et al. 2021) and (Bi et al. 2021) observed an improvement in the vertical accuracy of UAV photogrammetric project products using GNSS RTK techniques by including oblique images.

On the other hand, if the elevation range (difference between the maximum and the minimum elevation) of the site under study is wide, taking images from a constant elevation above mean sea level (AMSL) does not provide optimal image overlap (this can take very low values) for 3 D reconstruction and provide inconsistent GSD of images. A possible solution to avoid this would be to fly at a constant height above ground level (AGL) (Trajkovski et al. 2020; Zapico et al. 2021). This would contribute to the efficiency of the dense image matching algorithms used to calculate the dense 3 D point clouds. However, this implies having an adequate digital terrain model (DTM) to enable the UAV to maintain the fixed level AGL and the software that supports terrain information for mission planning. There are DTMs or DEMs at the worldwide, national or local levels (from previous surveys), which are available to plan an AGL flight. However, there may be problems with resolution or lack of updating, which can be dangerous for the safety of the UAV or may not be useful for achieving an accurate AGL flight as these DTMs do not include tall vegetation, obstacles and electric power lines. Software that allows AGL flights to be programmed from a user-supplied DEM is now available, for example, UgCS (https://www.ugcs.com/, accessed 14 January 2022). There is a standalone software (UgCS-Mapper, https://www.ugcs.com/mapper, accessed 14 January 2022) that allows creating a DEM from images taken in an initial flight with a geotag accuracy of fewer than 10 m and containing elevation values.

There are several works in the scientific literature where the adaptation of flight height to the terrain is mentioned, but no further specifics are offered about flight altitudes and their influence on the accuracy of the produced 3 D point cloud (Cook 2017; Rossini et al. 2018; Valkaniotis et al. 2018). The work of (Yang et al. 2018) studied the optimisation of flight routes for the reconstruction of DTM based on a procedure that assumes a constant UAV flight height. In (Pepe et al. 2018), an overview of the airborne mission planning of the current platforms and sensors is given, but the terrain-following planning mode is only mentioned.

The final accuracy of the 3 D point cloud produced by the photogrammetric project, as well as the validity of the comparison of clouds generated at different times or from different sensors, is conditioned by the georeferencing strategy and the number and distribution of GCPs. Temporal analysis of landform topography requires high accuracy of measurements and reproducibility of the methodology as differencing of digital surface models leads to error propagation. In (Clapuyt et al. 2016), a study area characterized by gently topography was surveyed with a UAV platform equipped

with a standard reflex camera, varying the focal length of the lens and location of GCPs between flights. They concluded that the survey accuracy of GCPs play an important role in preventing changes detected on a surface measured at different times from being due to the error made in measuring the GCPs. A similar objective was set in (De Marco et al. 2021), using three study sites with different morphologies. Among other factors, they studied the effect of the number of GCPs and the accuracy of the measurement of their coordinates, deriving the same conclusions as those obtained in (Clapuyt et al. 2016). Nowadays, thanks to UAVs equipped with onboard global navigation satellite system-real-time kinematic (GNSS RTK) receivers, the GCPs could be no longer needed as the camera stations at the time of exposure can be determined to centimetre accuracy and used to georeference the block and control its deformations. Related to this, (Štroner et al. 2021) and (Bi et al. 2021) observed a systematic elevation error that arises when using this technique, concluding that inclusion of oblique images decreases it significantly. In (Forlani et al. 2018) reached horizontal accuracy lower than 2 cm in UAV photogrammetric project using an onboard GNSS RTK. They also observed a bias in the vertical component and concluded that the inclusion of a single GCP significantly improved this bias.

In view of the above, it is necessary to deepen the knowledge of the influence that certain factors related to the planning of the photogrammetric flight, such as the type of flight (AMSL or AGL), image angle, or the overlap scenario, have on the quality of the 3 D point cloud obtained from the photogrammetric projects derived from the flights.

The main objective of this study is to evaluate the influence of the image angle, the values of frontal and side overlaps, and the type of flight (AMSL or AGL), on the accuracy of the dense 3 D point cloud yielded by UAV-SfM. Additionally, some recommendations are derived on what should be followed when planning a UAV-photogrammetric project on terrain with complicated geometry.

2. Material and Method

To achieve the proposed objective, ten flights were conducted, five in AMSL and five in AGL mode, in each of which a different camera angle was set with respect to nadir: 0° (nadir), 11.25°, 22.5°, 33.75° and 45°, all of them with a 90% of frontal and side overlap. By combining photographs of the different flights, 168 UAV-SfM photogrammetric projects were derived, with different combinations of frontal and side overlaps and camera angles. Furthermore, a 3 D point cloud was collected with a terrestrial laser scanner (TLS). All these 3 D point clouds were georeferenced using the same set of GCPs. With the TLS reference cloud, distance between this and each of those derived from the UAV-SfM projects calculated in every point allowed to have an error distribution on the whole study site and to derive mean and standard deviation statistics.

2.1. Study site

The study site is located in the Tabernas Desert, Southeast Spain (Figure 1A). The coordinates UTM (Zone 30, European Terrestrial Reference System 89 (ETRS89)) of the centre of this area are X = 548800 and Y = 4096425, and its extension is 10095 m^2. The elevation range is 32 m, varying from 228 to 260 m, and it shows a wide range of slopes oriented in all directions (Figure 1B). The selection of this site was based on its complex morphology as well as the absence of vegetation (Figure 1C).

2.2. Uav data acquisition

The images used in this study were collected using a DJI Phantom 4 Pro, a rotary-wing UAV with four rotors that integrates a camera with a of CMOS sensor of one inch size and 20 megapixels, and an f2.8/f11 wide-angle lens with an equivalent focal length of 24 mm. This UAV incorporates a

GNSS, combining GPS and GLONASS signals, and records geolocation with a hover accuracy range of ±1.5 m (horizontal) and ±0.5 m (vertical). Vertical accuracy reaches better value than horizontal accuracy due to the built-in barometer of the UAV. Furthermore, the camera is mounted on a three-axis gimbal with an accuracy of ±0.02°, which is able to take images between 0 (nadir) and 90° (https://www.dji.com/it/products/compare-consumer-drones?from=p4p-or-p4a, accessed 14 January 2022).

The whole study site was covered by 10 different autonomous flights, meaning that in each of them, the UAV followed a previously programmed and loaded path, consisting of several flight path lines oriented in the North-South (NS) direction, followed by flight path lines in the East-West (EW) direction. Both frontal and side overlaps were 90%. In order to study the effect of varying the distance of the camera to the terrain under study during flight, five of these 10 flights were executed in AMSL mode, whereas the other five were executed in AGL mode. In each of these five flights, a different camera angle was fixed: 0° (nadir), 11.25°, 22.5°, 33.75° and 45°. Flights with oblique angle alternated lines containing camera angles posed in opposing directions. Light and weather conditions did not vary significantly during the flights.

UAV flights were programmed using UgCS software (https://www.ugcs.com/, accessed 14 January 2022), which allows the configuration of both AMSL and AGL mode flights. Altitude in AMSL flights was fixed at 65 m above take-off level, whereas in the AGL flights, the altitude was fixed at 65 m above ground level. In order to provide a detailed digital elevation model to the UgCS software to define the AGL flights, a previous UAV-SfM photogrammetric project was carried out with the same UAV and 80 m flight altitude AMSL.

Prior to the UAV flights, eight targets were evenly arranged across the study area to be used as GCPs (Figure 1B). As shown in Figure 1B, the GCPs were located in the lower elevation zone, given the impossibility of accessing the higher elevation zones. Ideally, GCPs should have been placed at the higher elevations of the study site to determine their influence on the quality of the derived 3 D point cloud. The coordinates of these points were surveyed using rover and base GNSS receivers, model Trimble R6, working in post-processed kinematic (PPK) mode, and locating the base station within the range of 300 m away to all the measured points. According to the specifications of the manufacturer, an error of 5 mm + 1 ppm root mean square horizontal and 10 mm + 1 ppm root mean square vertical can be expected for the PPK measurements. Taking into account these specifications, maximum horizontal error for GCPs was 5.3 mm and vertical error was 10.3 mm.

2.3. Imaging processing

All photogrammetric projects were processed using the Pix4Dmapper, V 4.6.4, commercial software, which incorporates an algorithm based on SfM-MSV techniques. The complete workflow includes several processes, which can be divided into the following three main steps: 1. Initial Processing, 2. Point Cloud and Mesh, and 3. DSM, Orthomosaic and Index., but this study used only the dense 3 D points cloud. One process included in the first step is a self-calibrating bundle adjustment based on camera internal and external orientation parameters.

Images of each of the ten flights described in the previous section were separated into two sets, one containing those taken in NS direction and the other in EW direction. In order to emulate different overlaps for the set on the flights made (90% both frontal and side overlap, 90/90), some images were removed to obtain 90% frontal and 70% side overlaps (90/70); and 70% both frontal and side overlaps (70/70). In this way, one (two) image(s) was removed, with the next one in each line kept to obtain a frontal overlap of 80% (70%), and one (two) line(s) was removed, with the next one kept to obtain a side overlap of 80% (70%). Three types of photogrammetric projects were

processed: (1) projects composed of a single flight line (NS or EW); (2) projects composed of two flight path lines combined (NS and EW), and with the same camera angle for both flight path lines; and (3) projects composed of flight path lines combined (NS and EW), with nadir (0°) angle camera for one direction and another considered angle for the other direction. All of these combinations were processed for each camera angle (0°, 11.25°, 22.5°, 33.75° and 45°), overlap combination (90/90, 90/70, and 70/70), and type of flight (AMSL and AGL). Projects were named as follow:

Type 1: FLYT_AG_DI_FO/SO

Type 2: FLYT_AG_NS_EW_FO/SO

Type 3: FLYT_0_NS_AG_EW_FO/SO and FLYT_AG_NS_0_EW_FO/SO

Where:

FLYT: type of flight (AMS or AGL)

AG: camera angle (0°, 11.25°, 22.5°, 33.75° or 45°)

DI: flight direction (NS: North-South; EW: East-West)

FO: frontal overlap

SO: side overlap

In order to avoid the influence on the results of the error in marking GCPs, the eight GCPs described in the previous section were marked in all projects with 90/90 overlap and double flight path lines. Then images were removed to set up the projects described in Table 1. Once the images were removed, the photogrammetric project was processed using the settings shown in Table 2.

As flight altitude was fixed at 65 m, the theoretical GSD corresponding to the camera that was fitted to the UAV utilised was 1.77 cm x pixel^{-1}. However, this value varies due to the scale change in the images caused by the terrain relief and the camera angle in off-nadir flights. In the AMSL flights, the take-off point had an elevation of 230 m. Therefore, taking into account that terrain range elevation varied from 228 m to 260 m, the camera elevation (vertical distance to the ground) varied from 35 m (GSD = 0.95 cm x pixel^{-1}) to 67 m (GSD = 1.83 cm x pixel^{-1}). The effect caused by terrain relief is partially mitigated in AGL flights as the camera maintains the distance to the terrain on the flight line.

2.4. Reference cloud acquisition and processing

Reference cloud was derived from a TLS Trimble TX8. This TLS can capture points at a speed of one million per second, has a precision < 0.001 m at a scanned distance of 80 m, and points scanned at 30 m are 0.057 m spaced (https://geospatial.trimble.com/sites/geospatial.trimble.com/files/2019-03/Datasheet%20-%20Trimble%20TX8%20Laser%20Scanner%20-%20English%20USL%20-%20Screen.pdf, accessed 9 October 2021).

To scan the whole study site, the TLS was placed in five different locations (Figure 1B), trying to avoid, as far as possible, the appearance of gaps or hidden areas in the 3 D point clouds. Prior to the scan task, 18 TLS_GCPs were placed throughout the study site, and their coordinates were measured using the same methodology described for GCPs in section 2.2. Each of the five

generated clouds was imported into Trimble Business Center 5.40 software (https://geospatial.trimble.com/products-and-solutions/trimble-business-center, accessed 14 January 2022), and initial scan location was established by visual identification of three TLS_GCPs. Then, the clouds were exported in LAS format. Using CloudCompare, a fine individual georeferentation was performed, taking into consideration all TLS_GCPs included in each of the five clouds (it varied from TLS_GCPs). All clouds were merged into a single cloud, and it was georeferenced using the GCPs described in section 2.2. The root mean square error calculated from position of each GCP measured with GNSS and its position measured in the georeferenced TLS point cloud was 0.012 m. The merged cloud was clipped using the contour of the study site and filtered to fit the minimum distance between points in 0.002 m. The definitive reference cloud was derived from this merged cloud by extracting in a random manner the 10% of points, resulting in a cloud with around 18 million points.

2.5. Accuracy assessment

In order to assess the accuracy of the 3 D point clouds generated from each studied photogrammetric project, the freely available Multiscale Model to Model Cloud Comparation (M3C2) algorithm was used (Lague et al. 2013). It is offered as a plugin by the CloudCompare software (https://www.danielgm.net/cc/, accessed 14 January 2022). The M3C2 algorithm calculates the local differences between the reference cloud (described in the previous section) and the compared point cloud (those derived from the photogrammetric projects) relative to a local surface normal orientation following two different steps. The first step describes a user-defined diameter (called normal scale, D) that is used to calculate the normal orientation in the reference cloud. All points included in a sphere of diameter D and centre in the point under study are used to fit a plane, which defines the normal orientation. In the second step, a second user-defined diameter (called projection scale, d) is used to define a cylinder with diameter d and axis parallel to normal orientation, including the point under study. Furthermore, the height of the cylinder is defined (h). All points of both clouds are projected on the cylinder axis, giving two distributions of distances, with origins on the point under study. The mean of each distribution gives the average position of each cloud along the normal direction, and the standard deviations provide a local estimate of the point cloud roughness. The local distance between the two clouds is given by the distance between the two calculated means.

From all calculated local differences, a distribution function of the local differences can be obtained and their mean value and standard deviation can be calculated. This was done for each of the clouds generated in each of the 168 photogrammetric projects. On the one hand, the mean difference can be assimilated to the accuracy of the photogrammetric project 3 D points cloud, where the values closest to zero for this difference indicates better accuracy, and on the other hand, the standard deviation can be assimilated to the precision of the photogrammetric project 3 D points cloud. The normal scale (D) was set as 25 times the average local roughness calculated for the reference cloud by CloudCompare (D = 0.25 m) to ensure that the normal direction is unaffected by point cloud roughness. In addition, the projection scale was set to d = 0.15 m, and the height of the cylinder was set to h = 1 m.

3. Results

3.1. Single line flights (projects type 1)

3 D point clouds yielded from images collected along a single line flight orientation (NS or EW, photogrammetry projects type 1, as described in section 2.3) generally resulted in no full coverage of the study site and were not considered for analysis.

3.2. Double line flights and single-camera angle (projects type 2)

The absolute value of M3C2-calculated mean difference by comparing the type 2 photogrammetric projects with the reference cloud (Figure 2) showed a similar trend for most overlap scenarios and the types of flights studied (AMSL and AGL). Accuracy increased as the camera angle increased from the nadir orientation to camera angles 22.5° or 33.75°, where the best accuracy values were reached. Accuracy usually decreases for a camera angle of 45°.

According to Figure 2, in a direct comparison between AMSL and AGL projects for the different overlap scenarios and camera angles studied, AGL projects only improved the AMSL accuracy results in all studied angles for a 90/90 overlap.

The influence of the camera angle on the accuracy was greater for projects AMSL than for projects AGL, independently of the overlap scenario. The range of accuracy values for each AMSL overlap combination was 0.037 m, 0.024 m and 0.033 m for a 90/90, 90/70 and 70/70 overlap, respectively. For each AGL overlap combination, these ranges were 0.026 m, 0.013 m and 0.009 m, respectively, each lower than the corresponding ranges in AMSL projects. In addition, as shown in Table 3, the best accuracy results for the AMSL projects were 0.004 m for the 90/90 overlap and 33.75°, 0.001 m for 90/70 and 33.75°, and 0.001 m for 70/70 and 33.75°. For the AGL projects, the best accuracies were 0.0001 m for the 90/90 overlap and 22.5°, 0.011 m for 90/70 and 22.5°, and 0.011 for 70/70 and 33.75°.

The standard deviation of distances between the reference TLS cloud and the clouds derived from projects type 2 (Figure 3) did not show a clear trend or difference between AMSL and AGL projects. For most projects studied, the best precision values were obtained for camera angles ranging from 11.25° to 33.75° for any combination of overlap and kind of flight.

As shown in Table 3, for the 90/90 overlap scenario, the best precision value for AMSL projects was found using a camera angle of 33.75° (0.063 m). This value was also the best for AGL projects with camera angles of 11.25° and 33.75°. For the 90/70 overlap, the best precision values were found for 22.5° (0.064 m) in AMSL flights, and 11.25° and 33.75° (0.065 m), in AGL flights. Finally, for the 70/70 overlap, the AMSL flights reached the best precision at camera angles 11.25° and 22.5° (0.066 m), whereas the AGL flights found it at a camera angle of 33.75° (0.065 m).

The influence of the camera angle in precision was very similar for most cases, independently of the overlap scenario. The standard deviation or precision variation range for most AMSL and AGL projects was around 0.004 m for the 90/70 and 70/70 overlap scenarios. For the 90/90 overlap scenario, the variation range was 0.017 and 0.002 m for AMSL and AGL flights, respectively, indicating that for AGL flights with a 90/90 overlap, the camera angle barely affected the precision of the projects carried out.

Most overlap and flight combinations yielded the best accuracy and precision values for camera angles of 22.5° or 33.75°. GSD values of AMSL projects were directly related with precision values (the higher the GSD value the better the accuracy), contrary to was observed for AGL, where no relationship was observed (Table 3).

By studying separately the positive and negative components of the M3C2-calculated distances between the reference TLS cloud and those corresponding to projects type 2 (same camera angle in both flight path lines), it was found that positive distances were mainly concentrated in the steeper slope zones (see Figure 1), whereas negative distances were spread by all the study sites. A representation of this behaviour is shown in Figures 4 (AMSL flights) and 5 (AGL flights), for a nadir camera angle and overlap scenarios of 90/90 (row A), 90/70 (row B) and 70/70 (row C). From

the map of M3C2-calculated distances (left columns in Figures 5 and 6), the maps of the positive component (right column) showed that these values were concentrated in the steeper areas, while the negative values (middle column) were distributed over the whole study site. Furthermore, projects with accuracy values closer to zero (AMSL 90/70 and AGL 70/70) were related to distributions where positive and negative distance values were distributed all over the study site. Barring the AMSL_78_NS-EW_90/90 project, as the accuracy of the projects worsens, so did precision to the same extent.

Figures 6 (AMSL flights) and 7 (AGL flights) confirm the behaviour commented in the previous paragraph for projects type 2 with a 90/90 overlap scenario: both figures show that as the positive distance (right column) spread all over the study site, the accuracy improved. Negative values (middle column) were spread all over the study site in all cases.

3.3. Double line flights and different-camera angle (projects type 3)

The combination of images from flights using nadir camera orientation with those from flights using camera angles different to the nadir resulted in a clear improvement of the accuracy of AGL projects compared to AMSL for all overlap scenarios and camera angles studied as shown in Figure 8.

AMSL flights achieve the best accuracy for a camera angle of 33.75° for the 90/90 (0.016 m), and 70/70 (0.018 m) overlap scenario. In contrast, for the 90/70 overlap scenario, the best accuracy was attained for a camera angle of 22.5° (0.023 m), in close proximity to the accuracy found for 33.75° (0.024 m). In the case of AGL flights, the best accuracy reading was found for different camera angles depending on the overlap scenario: 0.014 m for 90/90 overlap and 11.25° camera angle, 0.009 m for 90/70 and 33.75° and 0.014 m for 70/70 and 22.5°.

Independent of the type of flight (AMSL or AGL), the use of the same camera angle in both flight path lines (NS and EW) yielded better accuracy values than those using different camera angles for each flight line, with the exception of AGL flights with 90/70 overlap.

Similar to the results obtained for the projects using the same camera angle for both flight path lines, the best precision values, as shown in the Figure 9, were found for camera angles 22.5° and 33.75°, except for AGL flights with 90/90 overlap, where the best accuracy was obtained for 11.25° (0.0645 m). The best precision value (0.064 m) was found for an AMSL flight with a 90/90 overlap and 33.75° camera angle. For 90/70 and 70/70 overlaps, the best values were found in AGL flights with 33.75° and 22.5°, respectively.

4. Discussion

Although there are numerous studies in the scientific literature regarding UAV-SfM on topographic surfaces with complex geometry, there is a need to deepen the knowledge of the influence that factors such as flight altitude, overlap, or camera angle have on the quality of the generated 3 D point cloud. The objective of this work has been focused precisely on the study of the influence of the image angle, the values of frontal and side overlaps, and the type of flight (AMSL or AGL) on the accuracy of the dense 3 D point cloud yielded by UAV-SfM, evaluating 168 3 D point clouds derived from UAV-SfM projects carried out on a complex geometry terrain. A 3 D point cloud generated by a TLS was used as a reference for this evaluation, where the data is highly accurate, with a low error in its georeferencing. Furthermore, the comparison between the 3 D point clouds was performed by calculating the distance in the direction normal to the reference cloud, using the algorithm developed in M3C2, which is more suitable than the calculation of the vertical distance.

4.1. Double line flights and single camera angle (projects type 2)

In (Nesbit & Hugenholtz 2019), the quality of 3 D point clouds created with UAV-SfM was studied using AMSL flights and nadir camera angles, angles different to the nadir (from 0° to 35°), and off-nadir images (from 5° to 35°, they did not include larger angles than 35° in their study) as well as the nadir image set. They concluded that precision and accuracy achieved with angles between 20° and 35° were better than that attained with lower oblique angles (from 5° to 15°). This finding was in partial agreement with the results found in our work for projects including the same camera angle for both NS and EW flight path lines, even the nadir orientation. Our best accuracy results in projects with the same angle for NS and EW flight path lines were 22.50° (AGL_22.5_NS-EW_90/90) and 33.75° (AMSL_33.75_NS-EW_90/70, Figure 2). In contrast, the camera angle did not significantly influence precision (Figure 3). (Smith & Vericat 2015) found the worst accuracy results in projects with nadir imagery taken from UAVs, compared to projects with non-nadir imagery obtained from the ground or a manned gyrocopter, although it does not provide an optimal angle value. This behaviour is similar to that found in our work, where the general tendency for projects using images with the same angle on the NS and EW flight path lines was to show the worst accuracy and precision values for the nadir angle. However, it should be noted that for an angle of 45°, the quality of the 3 D point cloud worsens again, which should be considered when flying manually or taking images physically from the ground, where the camera angle is more difficult to control. The main goal of the research of (Ostrowski 2016) was to set and empirically verify the accuracy of measurements in oblique aerial images in an urban area. Although the only angle studied was 45° − one of the worst performers in our study − the results showed high accuracy for the products derived from the UAV-SfM projects.

AGL flights substantially improved the accuracy with respect to the AMSL flights in all overlap combinations for nadir and 11.25°. There was no accuracy improvement for larger angles (from 22.5° to 45°). Even the AMSL flights yielded better accuracy than the AGL ones. This is not in agreement with that reported in (Zapico et al. 2021), who using a camera angle of 40° reported better accuracy values in AGL flights than in AMSL flights.

Differences in precision between AGL and AMSL flights were not as evident regarding accuracy. Only for the nadir projects the values were better for AGL flights than AMSL ones. This trend was observed for all overlap combinations. For the rest of the angles, no substantial differences in precision existed between AMSL and AGL flights. This is in partial agreement with the results reported by (Zapico et al. 2021), which showed an improvement in the accuracy of AGL flights over AMSL flights in both nadir and 40° image angle projects.

No significant differences in accuracy and precision values were found among the different overlap combinations. Only a slight improvement in accuracy values was observed for AGL flights with a combination of 90/90 overlaps. Contrary to these results, (Rupnik et al. 2015; Gerke et al. 2016) concluded that an increase in the overlap between images in airborne photogrammetry projects improves the precision and helps in compensating for deficits of image calibration. Similar to our results were those reported in (Nesbit & Hugenholtz 2019) regarding working with UAV-SfM projects over complex terrain geometry, where an increase in 3 D point cloud accuracy was found when moving from a 70/70 to a 90/70 overlap. However, when increasing to a 90/90 overlap, the accuracy decreased for practically all the scenarios studied. With respect to precision, the best results for all camera angles studied were found for a 70/70 overlap and the worst for 90/70 and 90/90 overlaps. In any case, the differences in accuracy or precision between the different overlaps were not very noticeable. Our best accuracy value was observed in the AGL_22.5°_NS-EW_90/90 project. Precision values from 11.25° to 33.75° were practically equalled in AMSL and AGL flights.

The spatial distribution of the M3C2 distance (Figures 4 to 7) showed a systematic error that was also reported in previous work (e.g., (James & Robson 2014; Nesbit & Hugenholtz 2019; James et al. 2020)), described as the 'dome effect'. Our results showed negative M3C2 differences (the 3 D UAV-SfM point cloud below the TLS cloud) spread over the whole study surface. Positive differences (the 3 D UAV-SfM point cloud above the TLS cloud) were found in the steep slope areas of the study site, as evident in the central columns of Figures 4 (AMSL flights) and 5 (AGL flights) for the case of nadir angles and each combination of overlaps considered. Figures 6 (AMSL flights) and 7 (AGL flights) showed positive differences in the steep slope areas as well for the 90/90 overlaps and each image angle studied (the rest of the projects not shown had the same trend). The improvement of the accuracy values is related to widening the distribution of positive values of the M3C2 distance over the whole study site, thus cancelling the 'dome effect'. For example, each project considered in Figure 4 (AMSL flights) has its equivalent in Figure 5 (AGL flights), which improves accuracy and, to a lesser extent, precision. It is also observed that the equivalent in Figure 5 of each project in Figure 4 presents a distribution of the positive values of the M3C2 distance with a wider spread over the entire study area, whereas the spatial distribution of the negative values does not vary substantially. These results are in agreement with those found in (Nesbit & Hugenholtz 2019), who observed the reduction or elimination of the dome effect when including oblique images in UAV-SfM photogrammetric projects.

4.2. Double line flights and different camera angle (projects type 3)

The trend of accuracy values for the projects where the flight line in one direction used nadir images and off-nadir in the other direction was similar to projects where the angle was the same for both directions: the general trend was to obtain the best accuracy values when images with an angle of 22.5° or 33.75° were combined with the nadir images in one direction. Consistent with these results, the works of (Štroner et al. 2021) and (Bi et al. 2021) concluded that accuracy improved when UAV photogrammetric projects with nadir images included some oblique images. In particular, (Štroner et al. 2021) combined vertical images with images with an angle of 15° on one side and a 30° on the other, obtaining the best results (worst systematic error not exceeding 0.03 m) in the second case. The research by (Bi et al. 2021) covered the study area with vertical images and added 45° angled images taken from the last waypoint of the initial route to the centre of the study area. They concluded that by adding a small number of oblique images the elevation accuracy improved significantly. However, in (Zapico et al. 2021) it was found that the combination of nadir and oblique images improved accuracy over nadir-only projects but worsened over oblique-only projects.

AGL flights generally had M3C2 distances closer to zero than AMSL flights, which is in line with (Trajkovski et al. 2020), who propose AGL flights to obtain optimal accuracies in steep terrain. Precision did not result in such a clear trend for these same angles, with the best values appearing at the 90/90 overlaps of the AMSL and AGL flights. In (Amrullah et al. 2016) also obtained better precision and accuracy values when combining nadir images and off-nadir (42°), which is in partial agreement with those found in this work, where only the improvement of the accuracy was related to the use of nadir and off-nadir images.

Previous works suggested that oblique images should account for approximately 10% of the nadir images (e.g., (Carbonneau & Dietrich 2017; Nesbit & Hugenholtz 2019)) as a higher proportion means poorer results. In our work, where the results do not match those, the projects that have combined nadir and oblique images have included 50% of each type. Compared to those with 100% oblique images (previous section), the accuracy and precision values were slightly better when 100% of the images were oblique. We, therefore, agree with (Nesbit & Hugenholtz 2019), who argue that more rigorous research into the impact of oblique image proportions within a given image block is warranted.

AGL flights improved accuracy over AMSL flights regarding the entire range of angles studied and all overlap combinations. The differences were not so noticeable for the angle 33.75° and the 90/90 and 70/70 overlaps. There was no direct influence of the type of flight considered on the precision achieved.

Although not represented, the distribution of the M3C2 distance over the study surface followed the same trend as that observed for projects with the same image angle in both directions of the flight path lines: for worse accuracy values, the positive distances are concentrated in the areas with the steepest slope, with the 'dome effect' appearing, and the negative distances are distributed over the whole study site. For projects with better accuracy, both positive and negative distances are spread over the entire study site.

Generally, the comparison of results obtained by projects using the same angle in both directions of the flight path lines (NS and EW, Figure 2) and those using a nadir camera orientation in one direction (NS or EW) and another angle in the other direction (EW or NS, Figure 8), shows that the former achieved better accuracy values (M3C2 mean distance values were practically zero). The latter demonstrated that the lowest M3C2 mean distance values did not fall below 0.010 m. In contrast, no differences were observed in the precision values (standard deviation of the M3C2 distances, Figures 3 and 9), with almost all of the best values found around 0.064 m. Therefore, from an accuracy point of view, it seems more appropriate to use oblique angles in both flight directions than to use a nadir angle in one direction of the flight path lines and an off-nadir angle in the other direction.

5. Conclusions

Planning UAV-SfM projects in terrain with complicated geometry and steep slopes requires several considerations that are not as critical when the terrain is flat. Only with flat terrain is it possible to obtain a 3 D point cloud with sufficient planimetric and altimetric accuracy.

In this type of terrain, imagery with an angle of 22.5° in both flight line directions (NS and EW), 90/90 overlap and AGL flight is the optimal combination for best accuracy and high precision.

Although not the best option, many UAV-SfM projects in the field of geosciences and surveying are planned with nadir imagery. In this case, the best results are obtained with AGL flights and a 90/70 overlap.

AGL flights require the prior existence of a DEM of the area under study. Since the existing DEMS may have a resolution and/or accuracy that is not adequate or terrain modifications are not registered, generating an ad hoc DEM from a set of images containing georeferencing data in their EXIF data is advisable. The GPS accuracy of the UAV will provide a suitable DEM for planning the final AGL flight.

AGL flights have been shown to affect the accuracy of UAV-SfM projects positively. Therefore, further research is warranted.

Acknowledgments

The authors would like to thank Delegación Territorial de Desarrollo Sostenible en Almería (Consejería de Agricultura, Ganadería, Pesca y Desarrollo Sostenible, Junta de Andalucía) for continued research access to the Paraje Natural Desierto de Tabernas. This research was supported by grant PPUENTE2021/003, from Universidad de Almería (Spain), co-financed with FEDER founds of the European Union. The first author Francisco Agüera-Vega was supported by the

Spanish Ministerio of Science, Innovation and Universities (reference PRX19/00236) for his study visit in the Department of Engineering (DIEF) 'Enzo Ferrari', University of Modena and Reggio Emilia, Modena, Italy, where part of this work was developed.

References

Agüera-Vega F, Carvajal-Ramírez F, Martínez-Carricondo P, Sánchez-Hermosilla López J, Mesas-Carrascosa FJ, García-Ferrer A, Pérez-Porras FJ. 2018. Reconstruction of extreme topography from UAV structure from motion photogrammetry. Meas J Int Meas Confed. 121(February):127–138.

Amrullah C, Suwardhi D, Meilano I, Engineering G, Sensing R, Forum Y, Camera V. 2016. PRODUCT ACCURACY EFFECT OF OBLIQUE AND VERTICAL NON-METRIC DIGITAL CAMERA UTILIZATION IN UAV-PHOTOGRAMMETRY TO DETERMINE FAULT PLANE. III(July):12–19.

Ao T, Liu X, Ren Y, Luo R, Xi J. 2018. An approach to scene matching algorithm for UAV autonomous navigation. In: 2018 Chinese Control Decis Conf. [place unknown]; p. 996–1001.

Bemis SP, Micklethwaite S, Turner D, James MR, Akciz S, T. Thiele S, Bangash HA. 2014. Ground-based and UAV-Based photogrammetry: A multi-scale, high-resolution mapping tool for structural geology and paleoseismology. J Struct Geol. 69(PA):163–178.

Bi R, Gan S, Yuan X, Li R, Gao S, Luo W, Hu L. 2021. Studies on Three-Dimensional (3D) Accuracy Optimization and Repeatability of UAV in Complex Pit-Rim Landforms As Assisted by Oblique Imaging and RTK Positioning. Sensors. 21(23):8109.

Carbonneau PE, Dietrich JT. 2017. Cost-effective non-metric photogrammetry from consumer-grade sUAS: implications for direct georeferencing of structure from motion photogrammetry. Earth Surf Process Landforms. 42(3):473–486.

Carricondo M, Sci H, Carricondo-Martínez P, Carvajal-Ramírez, Fernando Yero-Paneque L, Agüera-Vega F. 2021. Combination of HBIM and UAV photogrammetry for modelling and documentation of forgotten heritage . Case study : Isabel II dam in Níjar (Almería , Spain). Herit Sci [Internet].:1–15. https://doi.org/10.1186/s40494-021-00571-8

Carvajal-Ramírez F, Aguëra-Vega F, Martínez-Carricondo PJ. 2016. Effects of image orientation and ground control points distribution on unmanned aerial vehicle photogrammetry projects on a road cut slope. J Appl Remote Sens. 10(3).

Carvajal-Ramírez F, da Silva JRM, Agüera-Vega F, Martínez-Carricondo P, Serrano J, Moral FJ. 2019. Evaluation of fire severity indices based on pre- and post-fire multispectral imagery sensed from UAV. Remote Sens. 11(9).

Clapuyt F, Vanacker V, Van Oost K. 2016. Reproducibility of UAV-based earth topography reconstructions based on Structure-from-Motion algorithms. Geomorphology [Internet]. 260:4–15. http://linkinghub.elsevier.com/retrieve/pii/S0169555X15002652

Cook KL. 2017. An evaluation of the effectiveness of low-cost UAVs and structure from motion for geomorphic change detection. Geomorphology [Internet]. 278:195–208. http://dx.doi.org/10.1016/j.geomorph.2016.11.009

Ferrer-González E, Agüera-Vega F, Carvajal-Ramírez F, Martínez-Carricondo P. 2020. UAV photogrammetry accuracy assessment for corridor mapping based on the number and distribution of ground control points. Remote Sens. 12(15).

Fonstad MA, Dietrich JT, Courville BC, Jensen JL, Carbonneau PE. 2013. Topographic structure from motion: a new development in photogrammetric measurement. Earth Surf Process Landforms [Internet]. 38(4):421–430. http://doi.wiley.com/10.1002/esp.3366

Forlani G, Dall'Asta E, Diotri F, di Cella UM, Roncella R, Santise M. 2018. Quality assessment of DSMs produced from UAV flights georeferenced with on-board RTK positioning. Remote Sens. 10(2).

Furukawa Y, Ponce J. 2010. Accurate, dense, and robust multiview stereopsis. IEEE Trans Pattern Anal Mach Intell. 32(8):1362–1376.

Gerke M, Nex F, Remondino F, Jacobsen K, Kremer J, Karel W, Huf H, Ostrowski W. 2016. Orientation of oblique airborne image sets - Experiences from the ISPRS/Eurosdr benchmark on multi-platform photogrammetry. Int Arch Photogramm Remote Sens Spat Inf Sci - ISPRS Arch. 2016-Janua(September):185–191.

Gong C, Lei S, Bian Z, Liu Y, Zhang Z, Cheng W. 2019. Analysis of the Development of an Erosion Gully in an Open-Pit Coal Mine Dump During a Winter Freeze-Thaw Cycle by Using Low-Cost UAVs. Remote Sens. 11(11):1356.

Harwin S, Lucieer A, Osborn J. 2015. The impact of the calibration method on the accuracy of point clouds derived using unmanned aerial vehicle multi-view stereopsis. Remote Sens. 7(9):11933–11953.

James MR, Antoniazza G, Robson S, Lane SN. 2020. Mitigating systematic error in topographic models for geomorphic change detection: accuracy, precision and considerations beyond off-nadir imagery. Earth Surf Process Landforms. 45(10):2251–2271.

James MR, Robson S. 2014. Mitigating systematic error in topographic models derived from UAV and ground-based image networks. Earth Surf Process Landforms. 39(10):1413–1420.

Lague D, Brodu N, Leroux J. 2013. Accurate 3D comparison of complex topography with terrestrial laser scanner: Application to the Rangitikei canyon (N-Z). ISPRS J Photogramm Remote Sens. 82(February 2013):10–26.

Mancini F, Dubbini M, Gattelli M, Stecchi F, Fabbri S, Gabbianelli G. 2013. Using Unmanned Aerial Vehicles (UAV) for High-Resolution Reconstruction of Topography: The Structure from Motion Approach on Coastal Environments. Remote Sens [Internet]. 5(12):6880–6898. http://www.mdpi.com/2072-4292/5/12/6880/

Manconi A, Ziegler M, Blöchliger T, Wolter A. 2019. Technical note: optimization of unmanned aerial vehicles flight planning in steep terrains. Int J Remote Sens [Internet]. 40(7):2483–2492. https://doi.org/10.1080/01431161.2019.1573334

De Marco J, Maset E, Cucchiaro S, Beinat A, Cazorzi F. 2021. Assessing repeatability and reproducibility of structure-from-motion photogrammetry for 3d terrain mapping of riverbeds. Remote Sens. 13(13).

Martínez-Carricondo P, Agüera-Vega F, Carvajal-Ramírez F. 2020. Use of UAV-photogrammetry for Quasi-vertical wall surveying. Remote Sens. 12(14).

Menegoni N, Giordan D, Perotti C. 2020. Reliability and uncertainties of the analysis of an unstable rock slope performed on RPAS digital outcrop models: The case of the gallivaggio landslide (Western Alps, Italy). Remote Sens. 12(10).

Mourato S, Fernandez P, Pereira L, Moreira M. 2017. Improving a DSM Obtained by Unmanned Aerial Vehicles for Flood Modelling. IOP Conf Ser Earth Environ Sci. 95(2).

Nesbit PR, Hugenholtz CH. 2019. Enhancing UAV-SfM 3D model accuracy in high-relief landscapes by incorporating oblique images. Remote Sens. 11(3):1–24.

Ostrowski W. 2016. Accuracy of measurements in oblique aerial images for urban environment. Int Arch Photogramm Remote Sens Spat Inf Sci - ISPRS Arch. 42(2W2):79–85.

Pepe M, Fregonese L, Scaioni M. 2018. Planning airborne photogrammetry and remote-sensing missions with modern platforms and sensors. Eur J Remote Sens [Internet]. 51(1):412–435. https://doi.org/10.1080/22797254.2018.1444945

Pérez M, Agüera F, Carvajal F. 2011. Digital camera calibration using images taken from an unmanned aerial vehicle. In: Int Arch Photogramm Remote Sens Spat Inf Sci - ISPRS Arch. Vol. 38. [place unknown].

Rossi G, Tanteri L, Tofani V, Vannocci P, Moretti S, Casagli N. 2018. Multitemporal UAV surveys for landslide mapping and characterization. Landslides. 15(5):1045–1052.

Rossi P, Mancini F, Dubbini M, Mazzone F, Capra A. 2017. Combining nadir and oblique uav imagery to reconstruct quarry topography: Methodology and feasibility analysis. Eur J Remote Sens [Internet]. 50(1):211–221. https://doi.org/10.1080/22797254.2017.1313097

Rossini M, Di Mauro B, Garzonio R, Baccolo G, Cavallini G, Mattavelli M, De Amicis M, Colombo R. 2018. Rapid melting dynamics of an alpine glacier with repeated UAV photogrammetry. Geomorphology [Internet]. 304:159–172. https://doi.org/10.1016/j.geomorph.2017.12.039

Rupnik E, Nex F, Toschi I, Remondino F. 2015. Aerial multi-camera systems: Accuracy and block triangulation issues. ISPRS J Photogramm Remote Sens [Internet]. 101(60):233–246. http://dx.doi.org/10.1016/j.isprsjprs.2014.12.020

Smith MW, Vericat D. 2015. From experimental plots to experimental landscapes: Topography, erosion and deposition in sub-humid badlands from Structure-from-Motion photogrammetry. Earth Surf Process Landforms. 40(12):1656–1671.

Štroner M, Urban R, Seidl J, Reindl T, Brouček J. 2021. Photogrammetry using UAV-mounted GNSS RTK: Georeferencing strategies without GCPs. Remote Sens. 13(7).

Trajkovski KK, Grigillo D, Petrovič D. 2020. Optimization of UAV flight missions in steep terrain. Remote Sens. 12(8):1–20.

Valkaniotis S, Papathanassiou G, Ganas A. 2018. Mapping an earthquake-induced landslide based on UAV imagery; case study of the 2015 Okeanos landslide, Lefkada, Greece. Eng Geol [Internet]. 245(November 2017):141–152. https://doi.org/10.1016/j.enggeo.2018.08.010

Westoby MJ, Brasington J, Glasser NF, Hambrey MJ, Reynolds JM. 2012. “Structure-from-Motion” photogrammetry: A low-cost, effective tool for geoscience applications. Geomorphology [Internet]. 179:300–314. http://linkinghub.elsevier.com/retrieve/pii/S0169555X12004217

Yang CH, Tsai MH, Kang SC, Hung CY. 2018. UAV path planning method for digital terrain model reconstruction – A debris fan example. Autom Constr [Internet]. 93(April):214–230. https://doi.org/10.1016/j.autcon.2018.05.024

Zapico I, Laronne JB, Mart F. 2021. Improvement of Workflow for Topographic Surveys in Long Highwalls of Open Pit Mines with an Unmanned Aerial Vehicle and Structure from Motion.

Table 1. Summarises the photogrammetric projects studied in this work.

	Overlap	Type of flight	Camera angle
(1) Single flight line (NS or EW)	90/90, 90/70, or 70/70	AMSL or AGL	0°, 11.25°, 22.5°, 33.75° or 45°
(2) Double flight path lines (NS and EW)	90/90, 90/70, or 70/70	AMSL or AGL	0° in one direction and 11.25°, 22.5°, 33.75° or 45° in the other direction
(3) Double flight path lines (NS and EW)	90/90, 90/70, or 70/70	AMSL or AGL	The same angle (0°, 11.25°, 22.5°, 33.75° or 45°) in both directions

Table 2. Settings of processing options in Pix4Dmapper for all processed photogrammetric projects.

Pix4Dmapper Step	Processing Option	Setting
1. Initial project processing	General/Keypoint Image Scale	Full
	Matching/Matching Image Pairs	Aerial Grid o Corridor Method: Standard
	Calibration/TargetedNumber of Keypoints	Automatic
	Calibration/Calibration	Standard
	Calibration/Rematch	All Internal and External Parameters Optimization
	Calibration/Export	Rematch: Automatic Automatic Camera Internals and Externals, AAT, BBA (AAT: automatic aerial triangulation; BBA: bundle block adjustment)
2. Point cloud and mesh	Point Cloud/Image Scale	½ (Half image size, Default)/Multiscale
	Point Cloud/Point Density	Optimal
	Point Cloud/Minimum Number of Matches	3
	Advanced/Matching Window Size	7×7 pixels

Table 3. Configurations that yielded the best accuracy values for single-camera angle projects.

Ovelap	Kind of flight	Camera angle (°)	Accuracy (m)	Precision (m)	GSD(cm)
90/90	AMSL	33.75	0.004	0.063	1.66
	AGL	22.5	0.0001	0.064	1.78
90/70	AMSL	33.75	0.001	0.065	1.65
	AGL	22.5	0.011	0.066	1.80
70/70	AMSL	33.75	0.001	0.067	1.69
	AGL	33.75	0.011	0.065	1.98

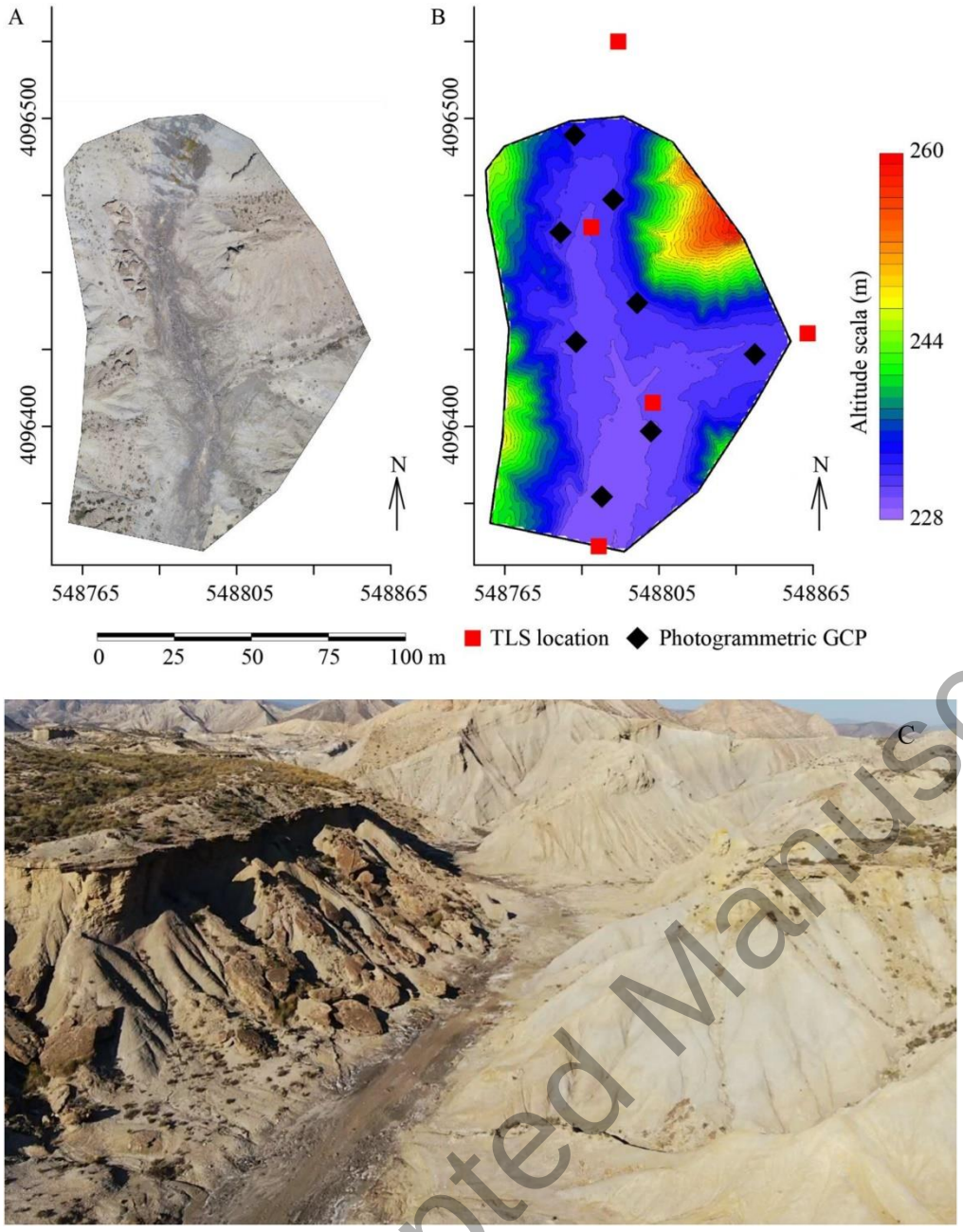

Figure 1. (A) Study site location; **(B)** scale colour contour map with TLS and ground control points (GCPs) of photogrammetric projects location. Coordinates refer to UTM (Zone 30, European Terrestrial Reference System 89 (ETRS89), (EGM08 geoid model); (**C) panoramic view of the site of study**.

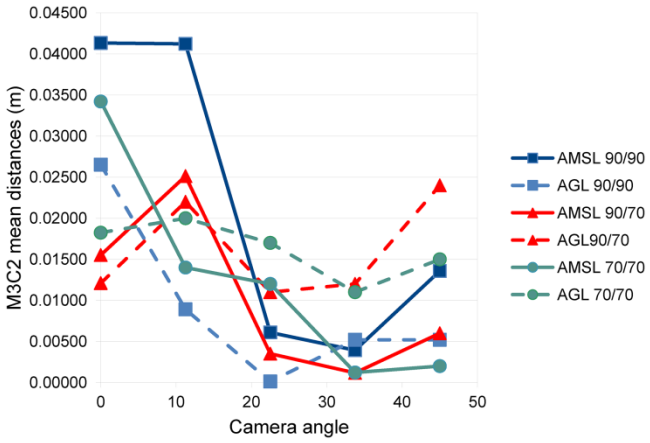

Figure 2. M3C2-calculated mean difference between TLS reference cloud and clouds obtained from different UAV-SfM image configurations: same camera angle for both flight directions (NS and EW), AMSL and AGL flights, and 90/90, 90/70, and 70/70 overlap configurations.

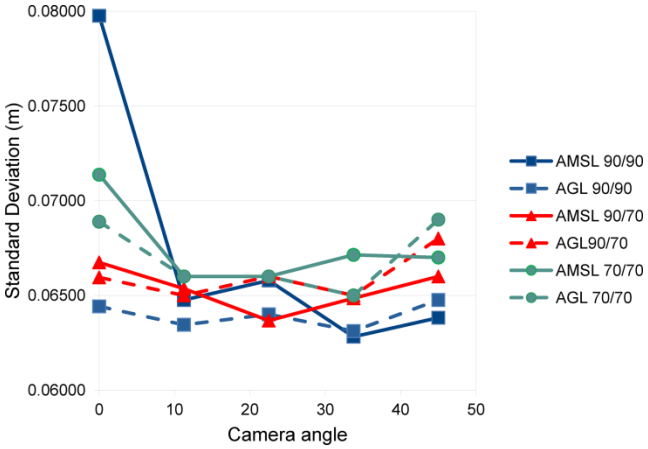

Figure 3. The standard deviation of M3C2-calculated distances between TLS reference cloud and clouds obtained from different UAV-SfM image configurations: same camera angle for both flight directions (NS and EW), AMSL and AGL flights, and 90/90, 90/70, and 70/70 overlap configurations.

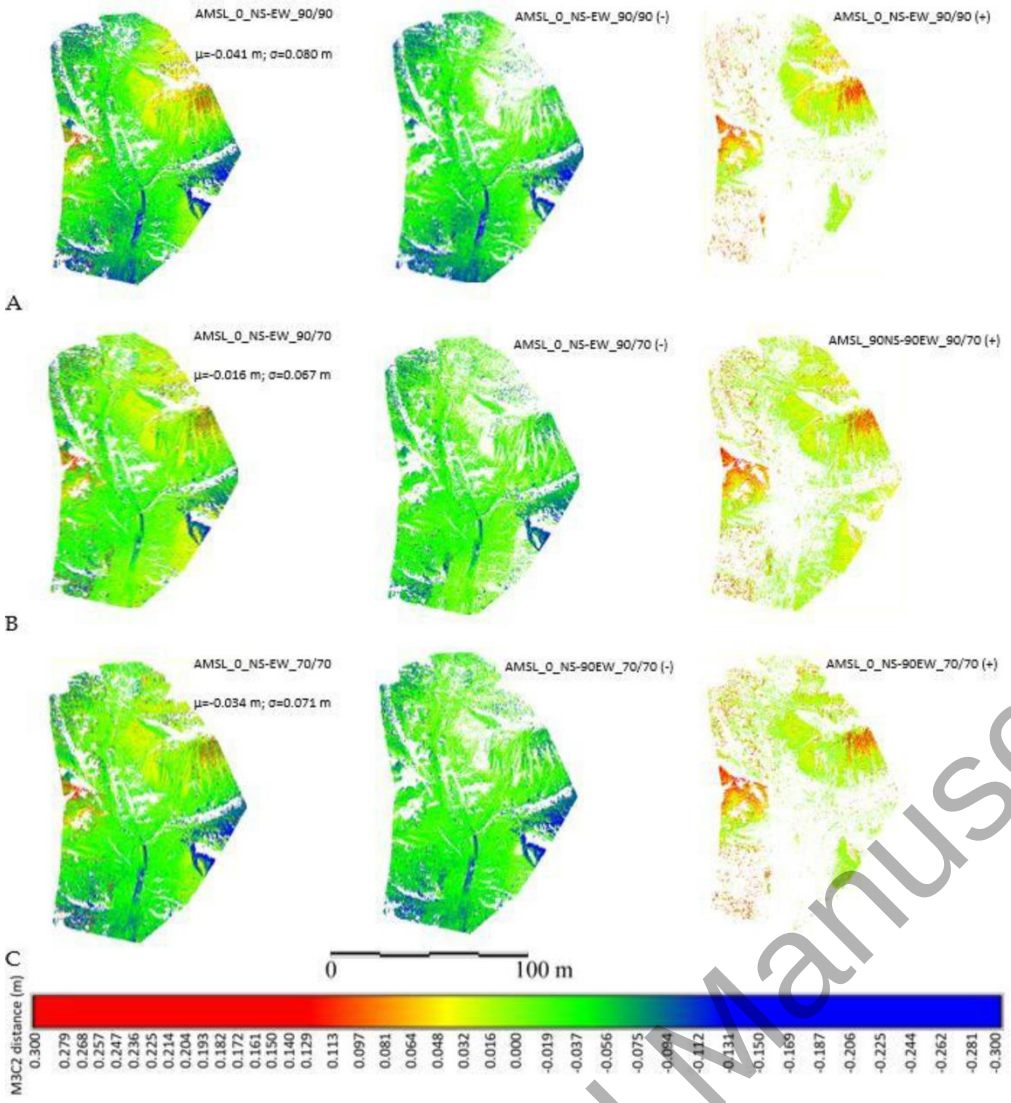

Figure 4. M3C2-calculated distances between TLS reference cloud and clouds obtained from project configurations using a nadir camera orientation for both flight directions (AMSL_0_NS-EW), following an AMSL flight and for different overlap scenarios (90/90, 90/70 and 70/70, rows A, B and C, respectively). The left column represents the distribution maps of all the points. The middle column represents the distribution of points where distances acquire negative values, and the right column shows where positive distance has been measured. Dimensions in the colour scale are m.

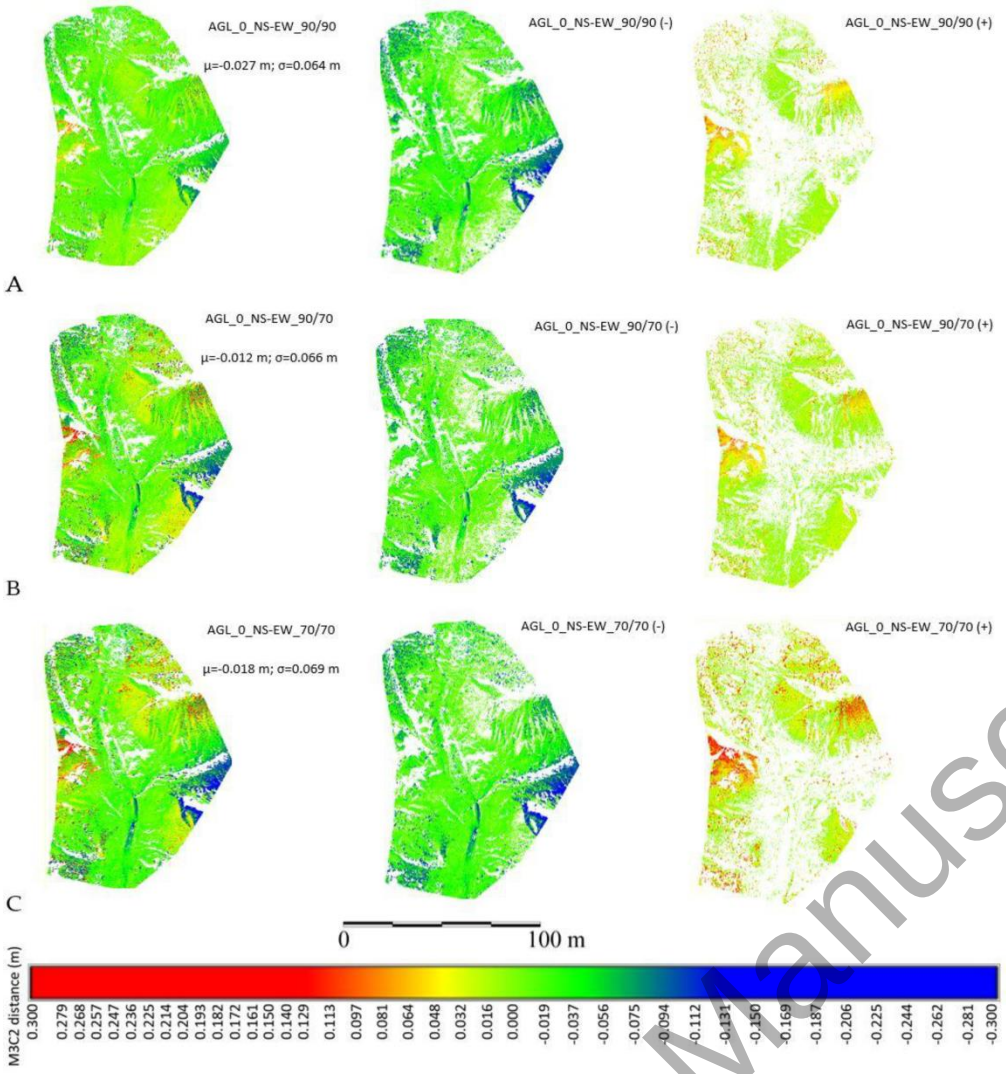

Figure 5. M3C2-calculated distances between TLS reference cloud and clouds obtained from project configurations using a nadir camera orientation for both flight directions (AGL_0_NS-EW_90/90), following an AGL flight and for different overlap scenarios (90/90, 90/70 and 70/70, rows A, B and C, respectively). The left column represents the distribution maps of all the points. The middle column represents the distribution of points where distances acquire negative values, and the right column shows where positive distance has been measured. Dimensions in the colour scale are m.

Figure 6. M3C2-calculated distances between TLS reference cloud and clouds obtained from project configurations using a single camera angle for both flight directions (0°, 11.25°, 22.5°, 33.75° and 45°), following an AMSL flight and for a 90/90 overlap scenario. The left column represents the distribution maps of all the points. The middle column represents the distribution of points where distances acquire negative values, and the right column illustrates where positive distance has been measured. Dimensions in the colour scale are m.

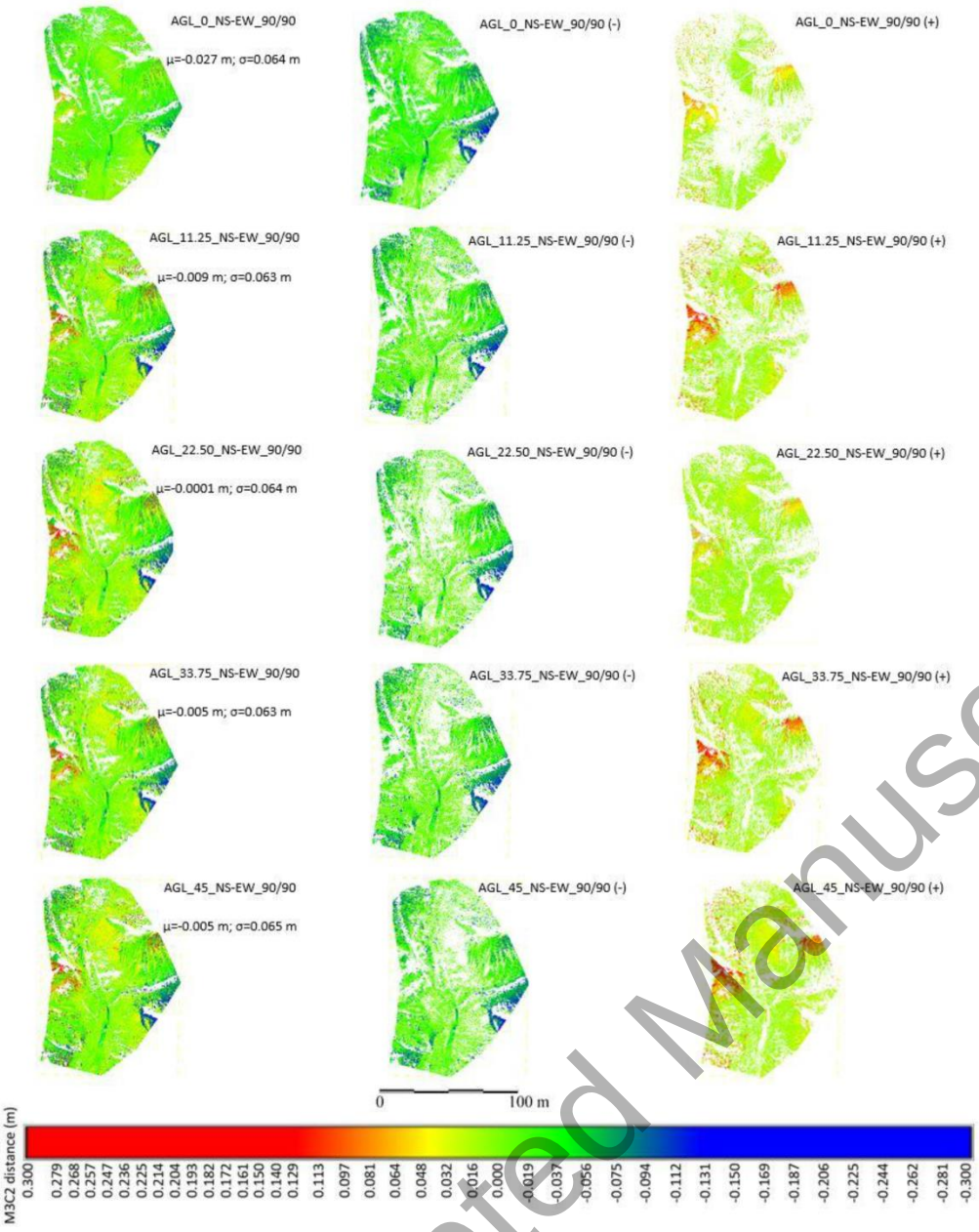

Figure 7. M3C2-calculated distances between TLS reference cloud and clouds obtained from project configurations using a single camera angle for both flight directions (0°, 11.25°, 22.5°, 33.75° and 45°), following an AMSL flight and for a 90/90 overlap scenario. The left column represents the distribution maps of all the points. The middle column represents the distribution of points where distances take negative values, and the right column demonstrates where positive distance has been measured. Dimensions in the colour scale are m.

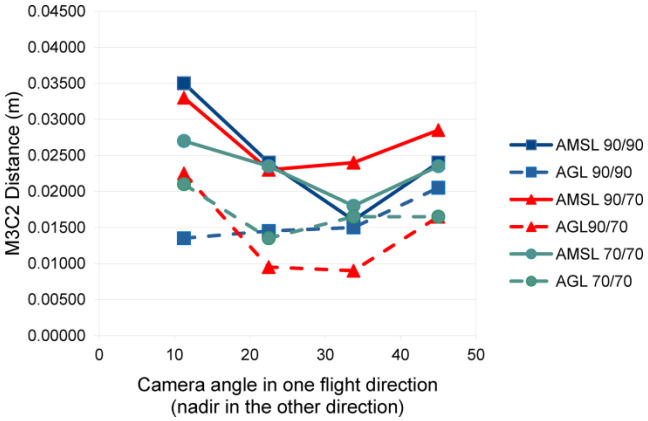

Figure 8. M3C2-calculated mean difference between TLS reference cloud and clouds obtained from UAV-SfM image configurations: nadir angle (0°) in one direction and 11.25°, 22.5°, 33.75° or 45° in the other flight direction; AMSL and AGL flights; and 90/90, 90/70, and 70/70 overlap configurations.

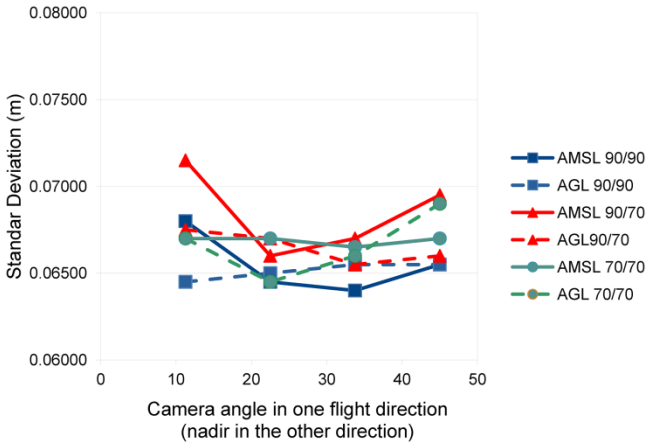

Figure 9. The standard deviation of M3C2-calculated distances between TLS reference cloud and clouds obtained from different UAV-SfM image configurations using a combination of both nadir in one flight line direction and no nadir camera orientation in the other flight line direction (11.25°, 22.50°, 33.75° and 45°).